SAND2019-15067R

Sandia National Laboratories

Operated for the U.S. Department of Energy
by National Technology and Engineering Solutions
of Sandia, LLC.

Albuquerque, New Mexico 87185

date: December 11, 2019

to: Distribution

from: Kyle Karlson, Guy Bergel, Org. 8752, MS-9042

subject: Hierarchical Multi-scale Modeling of Laser Weld Failure: An Initial Investigation

1 Introduction

The failure of 304L laser welds is of interest to system and component designers due to nuclear safety requirements for abnormal environments. Accurately modeling laser weld behavior in full system and component models has proven especially challenging due to three factors: the large variability observed in laser weld characterization tests; the difficulty in isolating the weld material for material characterization and modeling the weld material behavior; and the disparate scales associated with modeling laser welds in large systems. Recent work has shown that meso-scale geometric features of laser welds such as pores and weld root tortuosity are critical to accurately predicting the structural performance of welds. The challenge with modeling these welds is that the geometric features driving their structural performance are generally on the order of ten to hundreds of microns, but can affect the responses of interest in systems and components on the order of centimeters to meters.

Resolving these small scale laser weld features in larger scale engineering models is usually impractical, if not impossible. This is due to the fact that most weapons safety models are used to evaluate transient dynamic environments and require the interaction of components through contact to accurately simulate the scenario of interest. With the current state of production solid mechanics codes, this limits analysts to using explicit time integration to solve these problems. A major limitation of explicit analyses is that they are constrained by the Courant-Friedrichs-Lewy (CFL) condition for the explicit time step. The CFL condition is directly related to element size, and, as a result, analysts are severely limited in what geometric features they can resolve.

A customer interested in better predictions of laser weld failure requested models with a time step of approximately 50 nanoseconds or larger. With this time step requirement, the theoretical limit in element size is 155 microns. This is calculated using the time step limit equation provied by

the Sierra/SM Theory Manual [8] and commonly available material properties for stainless steel. Note that this is a theoretical limit and the SierraSM code scales the theoretical time step limit by 0.9 by default for to ensure stability. As a result, the practical smallest element length scale we can accommodate is approximately 175 microns. In an ideal scenario, if we are modeling a weld with a nominal weld depth of 0.030" (700 microns) we can only afford 4 elements through that weld for a full system or component model. Therefore, adequately resolving the pores and small scale geometry of the weld in order to produce accurate results is impossible even when using modeling techniques such as mass scaling and time scaling to circumvent the CFL condition.

Analysts are well aware of these limitations and have adopted two methods to attempt to predict laser weld failure in engineering scale models. The first method is that they use the base material plasticity properties in a mesh that resolves the general geometry of the weld as well as possible within their time step constraints. If time allows and data is available, they may assign the weld block its own element deletion criterion. This criterion is usually obtained through a rough calibration of the model to any available test data. The second method takes the first method one step further. In addition to tuning the failure criteria of the weld material, the analyst may calibrate a weld-specific material model for the weld block. Generally, they will calibrate the yield, hardening and failure criteria specific for the weld material and treat it separately from the surrounding base material. This type of calibration is almost always done with experimental data from tension tests of laser weld tension specimens. This sort of calibration can yield a material model parameter set for the weld material that is significantly different than the base material model parameter set. This is usually the case because the material model must account for geometric differences between the model and test specimen; and it must accomodate large discretization errors that arise due to the CFL time step constraint.

These weld modeling methods can lead to modeling errors when attempting to quantitatively predict laser weld failure. One factor contributing to the error is that the weld specimens that are tested for calibration can have much different geometries than those found in welded components. As a result, the apparent strength of the welds in the components of interest may be significantly different than the welds that were tested in a lab. Another potential contributor to error is that the loading conditions in the simulation environment of interest may be much different than the loading conditions of the test used to calibrate the model. As a result, the model may be extrapolating outside of the space in which it was calibrated.

2 Hierarchical Multiscale Method Overview

We propose using a hierarchical multiscale approach for modeling laser weld failure to overcome the issues mentioned in the end of section 1. The process begins by evaluating the welded component or system with the best coarse model possible in the environment of interest. Subvolumes in regions of interest in the component are then selected and a fine model is built inside those submodels. The fine subvolume models are then simulated using the resulting fields from the coarse model. This is done by interpolating the displacements from the coarse component model onto the boundaries of the subvolumes intersecting with the original model. The results from the fine subvolume models, such as the reactionary forces on the boundaries, are then used to recalibrate

the coarse model parameters. The coarse model can then be re-run using the updated coarse model parameters and the process can be repeated until the results converge as time allows.

The proposed approach is considered hierarchical because results from the fine model will be used to inform modeling decisions made in the coarse model. This is much different than coupled multiscale methods, such as Scharwz coupling [6, 2], where the fine models are directly coupled to the coarse model and both are evaluated concurrently. In general, coupled mutliscale models can produce more accurate results; however, they are also potentially more computationally expensive. In this approach, we sacrifice accuracy in order to reduce the cost of the coarse model.

The proposed method builds upon recent successes where we have developed a material model parameter set for vacuum arc remelted (VAR) 304L welds for quasistatic, room temperature environments. We have accurately predicted the failure behavior of welds using this material model by building meshes of detailed laser weld geometries acquired through micro-computed tomography scans [4]. Therefore, we confidence in predicting laser weld failure when high-fidelity models are used.

The goal is to use the coarse model as a *surrogate* model of the weld for the loading conditions of interest to the analyst assessing the weld behavior in a component or system model. This surrogate model of the weld will most likely only be valid for use in the particular problem being studied and should not be considered a general weld model. The validity of this approach requires the following assumptions to be true:

1. The initial coarse model deformation is close to what the deformation would be if a fine model was used for the entire simulation. In other words, the fields must be representative of those occurring on the finely-meshed model.
2. The fine model must contain all relevant physics to simulate the environment of interest. For 304L laser welds in abnormal environments, this includes geometry, rate- and temperature-dependent plasticity, and ductile damage.
3. Significant error is not introduced by the solutions produced in the coarse subvolume model.

In general, Items 1 and 3 precludes the use of under-integrated hexahedral elements for highly ductile materials as they have been shown to produce overly stiff results for problems with large plastic deformation. Item 2 is still currently being developed; however, we believe we have a validated model for 304L welds at room temperature[4].

Since we have a representative model for 304L welds which includes both void structure and constitutive parameters for damage and rate/temperature dependence, we plan to verify the proposed hierarchical multiscale method for a problem with a known solution. We will perform the verification as follows:

1. Evaluate several finely-meshed simulations of a component with different weld porosity realizations. The produced fields will be used as the 'truth' solution that we are trying to predict with the hierarchical multiscale approach.

2. Generate force-displacement data for laser weld tension specimens in a similar fashion to what is done for weld characterization. This will include generating samples and fine meshes of laser-welded tension specimens with voids, and simulating their response.

3. Calibrate an initial coarse model to the force-displacement curves from the simulations of the laser-welded tension specimen (Item 2) and predict the behavior of the component from Item 1 using the newly calibrated coarse model of the weld.

4. Extract subvolumes and boundary conditions from the coarse model of the component and evaluate the subvolume response using fine mesh realizations of porous welds.

5. Recalibrate the coarse model to the fine mesh subvolume results and predict the failure of the component.

In this memo, we execute this procedure once to show that the predictions of failure for a welded component improve using the hierarchical multiscale method compared to the traditional methods described earlier. The 'truth' verification problem we are evaluating is a pressurized can with welded lids. The weld has a constant weld cross-section but variable porosity. As a result of the porosity variability, several samples of the fine model were simulated with different void structures. Details on the verification simulation, material model, and void model are detailed in the sections that follow.

3 304L VAR Material Model Parameter Set for the Fine Models

The constitutive law used for all simulations is the DSA material model from Lamé in Sierra/SM [9]. The material parameters were calibrated to uniaxial tension data for 304L VAR material from [5] and other experimental sources within Sandia. The damage parameters were calibrated to notched tension and uniaxial tension data for 304L sheet also from [5]. MatCal was used for both calibrations.

The calibration was performed in a multi-step process. First, the plasticity parameters were calibrated to 304L VAR uniaxial tension force-displacement data taken at multiple rates. After that calibration was completed, a subset of the parameters was recalibrated until the model matched the 304L VAR data from [5] and literature data on 304L yield stress rate dependence [7]. Next, a separate plasticity model was calibrated to the 304L rolled sheet material concurrently to the notched and uniaxial tension data from [5]. After the plasticity model was calibrated for the sheet model, the damage model was calibrated to the same sheet data. All calibrations were performed using Dakota's SOGA and coliny_pattern_search algorithms. The final step of the calibration included scaling the damage model parameters with a constant scale factor to account for the small mesh size to be used in the fine models of the laser weld realizations. These scaled damage parameters were then copied into the material model parameter set for the 304L VAR material.

Note that this material model parameter set is representative of the 304L material we are modeling. The goal was to create a material parameter set that could be used to simulate the can crush test from [5]. This material parameter set has not been well validated and is calibrated to multiple

Table 1: Calibrated fine model DSA material model parameters

Material Parameter	Variable	Value	Units
Young's Modulus	E	200e9	Pa
Poisson's Ratio	ν	0.27	–
Density	ρ	7900	Kg/m^3
Rate independent yield constant	Y_0	182.7e6	Pa
Isotropic hardening constant	H	332.6e6	Pa
Isotropic dynamic recovery constant	R_d	2.883767751	–
Yield rate coefficient	f	2.33e-2	1/s
Yield rate exponent	n	15.15	–
Misorientation hardening modulus	ζ	0.1174576474	–
Misorientation hardening exponent	r	1	–
Plastic dissipation factor	β	0.9	–
Initial damage	ϕ_0	1e-4	–
Initial nucleated void size	v_0	2e-5	m^3
Initial void count per volume	η_0	5	$\frac{1}{m^3}$
Void growth exponent	m	0.657	–
Nucleation parameter 1	N_1	0.19856372987499998	–
Nucleation parameter 2	N_2	0	–
Nucleation parameter 3	N_3	1.6418203375	–

sources. However, this is of little importance to this study where we are using it as the basis for verification of the proposed hierarchical multiscale method. Since the material model is representative of 304L (*i.e* highly ductile, rate/temperature dependent, 304L informed damage model), the conclusions derived from the verification procedure outlined here are still valid.

The results from the 304L VAR plasticity parameter calibration are shown in fig. 1 and the results from the 304L sheet plasticity and damage calibration are shown in fig. 2. Note that temperature dependence was added to the initial yield stress parameter for this calibration. The temperature dependence function was taken directly from the MMPDS10 database [1] in Granta for 300 series stainless steels. All material parameters used for the fine models in this study are provided in table 1.

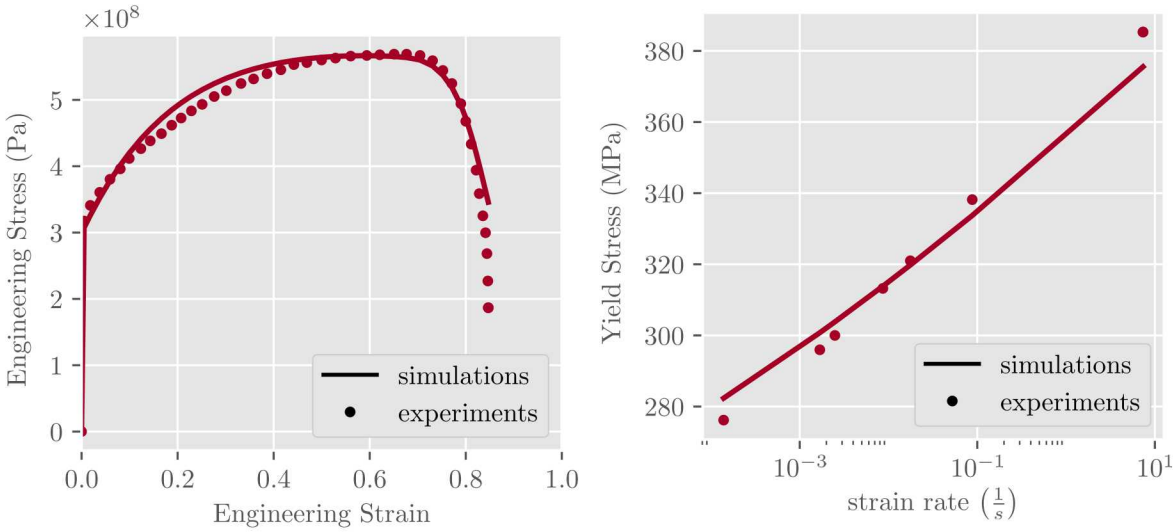

(a) 304L VAR uniaxial tension

(b) 304L yield stress rate dependence

Figure 1: The calibrated tension specimen results and yield stress versus strain rate curve are shown here for the 304L VAR material from [5]

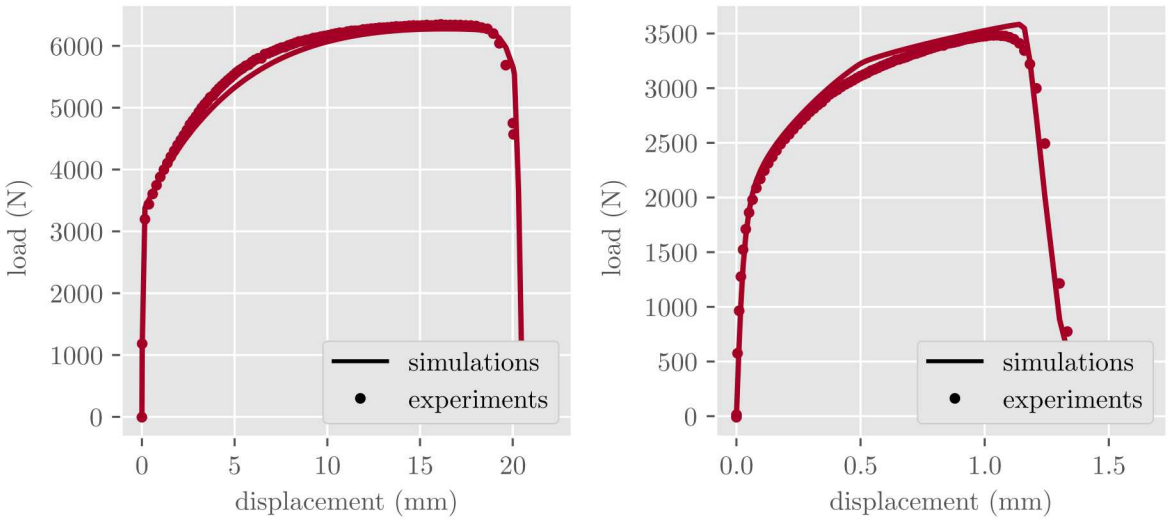

(a) 304L sheet uniaxial tension

(b) 304L sheet notched tension

Figure 2: The calibrated notched and uniaxial tension load-displacement curves are shown here for the 304L sheet material from [5]

4 Weld Porosity Model

Statistical characterization of the voids was conducted using available binarized CT scans of laser-welded tension specimens[4]. Several laser-welded specimens were scanned and they are identified with an 'S#' name. The specimens S24, S25, S26, S31, S32, and S33 were used to develop the

porosity model presented here. CT scanned void centroid locations, void sizes, and average weld depth were extracted from the series of scanned binarized images. To characterize the spatial location of the void centroids, each void was assigned a pair of coordinates indicating their distance orthogonal to the weld surface and weld plane, which are defined schematically in fig. 3.

The empirical distribution functions (EDFs) were constructed for the void centroid locations relative to the weld plane and surface as well as the effective spherical void radii, as shown in fig. 4. Note that the distance from the weld plane is unsigned, though the distribution is slightly skewed towards negative numbers. The precise reasoning for this trend is not currently known. For simplicity, the weld plane's orientation is assigned by the user, and is consistent for all geometries considered here.

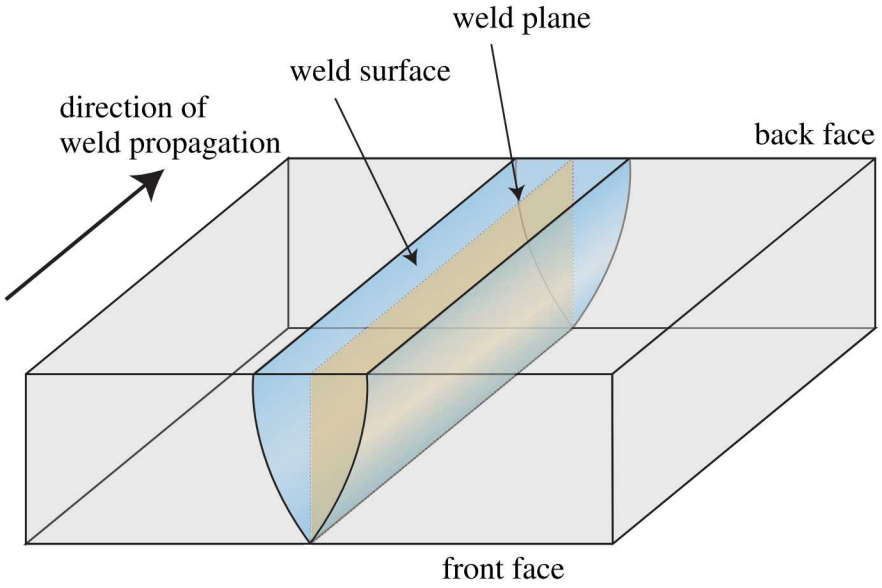

Figure 3: Schematic illustration of weld surface (top of weld, shown in blue) and weld plane (cut through weld, shown in orange)

The estimated CDF is constructed as a series of piecewise linear functions connected by the discrete data points of the EDF. With this assumption, the inverse transform sampling method is used to generate samples of voids within the welded region at locations relative to the weld plane/surface and with void radii whose estimated CDFs are known (which are assumed to be continuous and monotonically increasing). Cumulative probabilities are sampled from a uniform random distribution within the closed interval $[0.1, 0.99]$, which discounts outliers. In addition, voids whose locations are sampled outside of a user-specified width signifying the heat affected zone are also discounted, with the justification that the scale of the weld depth is proportional to the scale of distances of voids from the weld surface and plane as well. The sampled probabilities are subsequently mapped onto the set of realizations generated by the original random variable. With increasing sample size, the EDF of the samples asymptotically approaches that of the original CDF. In the current setting, voids are added until a target effective void volume per unit area along the weld plane is reached.

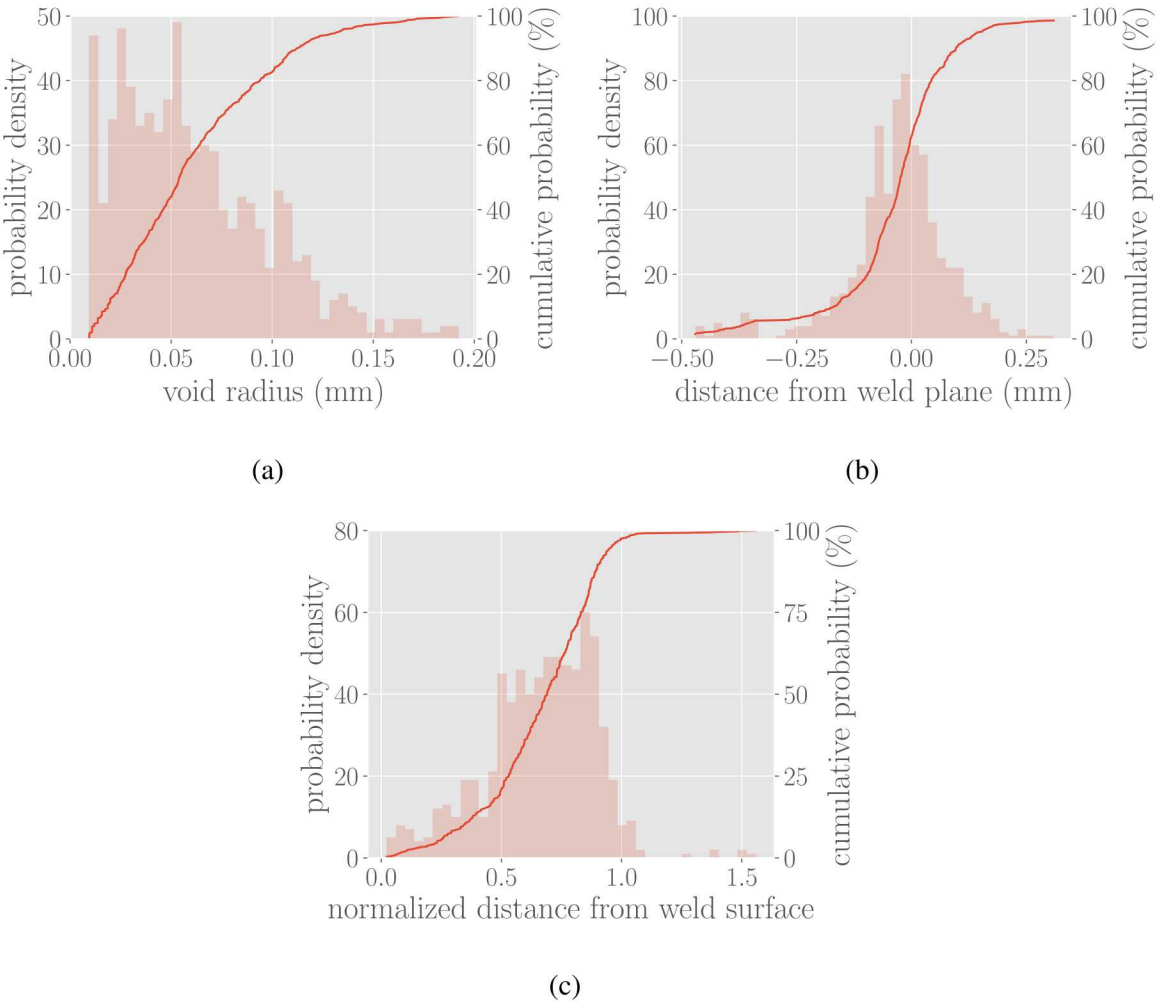

(a) (b)

(c)

Figure 4: EDFs for observed set of (a) void radii, (b) absolute distance from weld plane (discounting the first and last 10 outliers), and (c) distance from weld surface normalized by the average weld depth

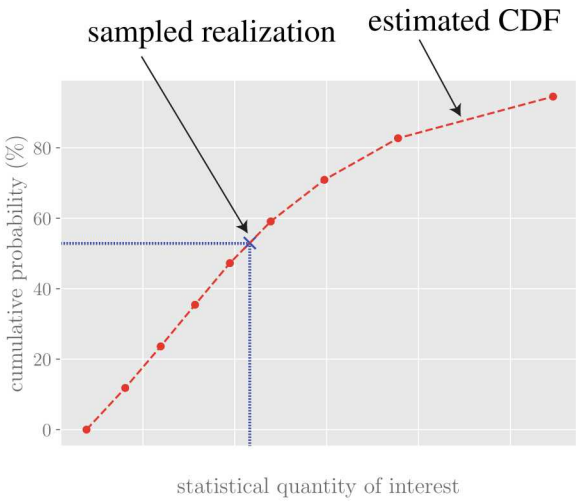

Figure 5: Schematic: Realization generated from inverse transform sampling of uniform cumulative probabilities using a piecewise linear approximation of CDF

5 Generated Weld Tension Data

A set of 10 samples of tension specimens was constructed using the procedure outlined in section 4. The tension specimen is 5.75” in length, 1” in width, and 0.09” in thickness. Additionally, the gage section is 2.5” long and 0.5” wide. The nominal weld depth was selected as 0.03”, which is representative of the assumed depth of the weld along the pressurized can which will be elaborated in section 6. The target void volume per unit weld plane was selected to be equivalent to that of specimen *S*26 which has a deep weld (1.63 *mm*) and a void density near the median of all samples. The estimated CDFs for the distance from weld plane/surface and void radius were taken from the combined data set containing all the specimen data. With the assumption that the void density is proportional to the nominal weld depth, the expected void density of the generated samples is approximately 46% that of specimen *S*26, as shown in the comparison of the weld cross-section of a single generated sample to that of *S*26 in fig. 6.

The voided geometries were meshed using CUBIT and SCULPT. The mesh for one of the generated samples is shown in fig. 7. The typical voided meshed tension specimen is composed of approximately 1*e*+06 hexahedral elements, with gradual refinement near the weld. The mesh at and near the weld is nearly uniform, with an element edge length of 30 μm. Elements near the voids were optimized to maintain a minimum scaled Jacobian of 0.4 by modifying node locations using SCULPT.

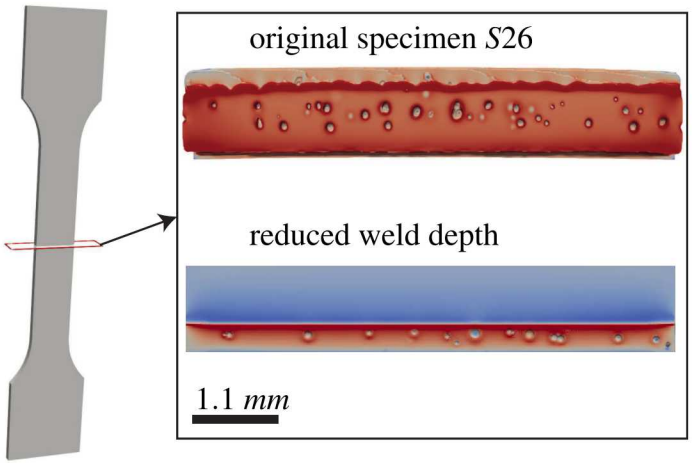

Figure 6: Comparison of voids along weld cross-section of the original specimen *S*26 (top) and the modified specimen with a reduced weld depth (bottom). Contour coloring is only used to highlight void locations.

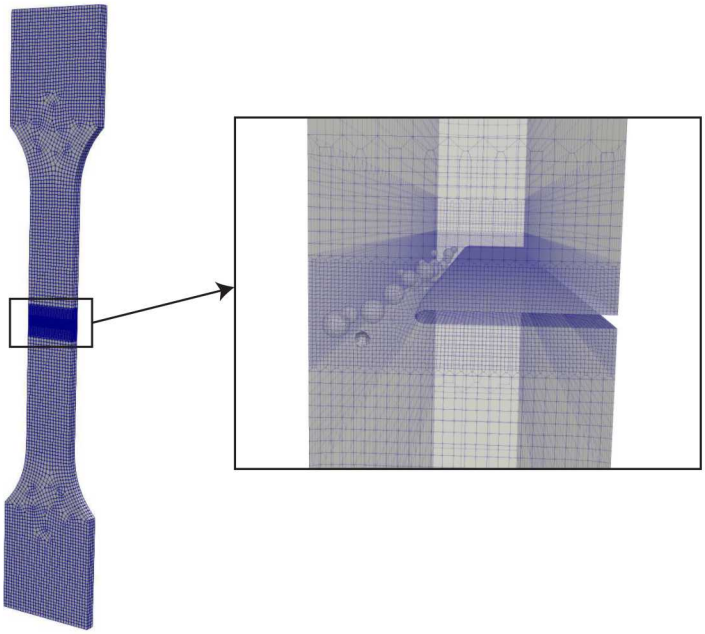

Figure 7: Overview of tension specimen mesh (left) and mesh along weld with external surfaces shown as translucent (right)

Physics simulations were conducted for each of the 10 generated samples using Sierra/SM. The constitutive law used to represent to the material response is based on a phenomenological plasticity model termed dynamic strain aging (DSA) [3]. The material parameters were set to those representative of 304L stainless steel for both the weld and base material. Due to this assumption, there is no distinct boundary between the weld region and the heat affected zone, as well as

between the heat affected zone and the base material. The region where the voids are contained is effectively the weld zone. The selective deviatoric element formulation was used. Element death/deletion was used to simulate fracture and crack propagation.

The specimens were loaded in tension until a sufficient amount of elements were removed to create a full breach along the entire depth of the weld. An example of a simulated failed tension specimen is shown in fig. 8. The reactionary force on the end grips is plotted against the relative displacement at the locations of the top/bottom extensometers (coinciding with their locations in the experiments) in fig. 9.

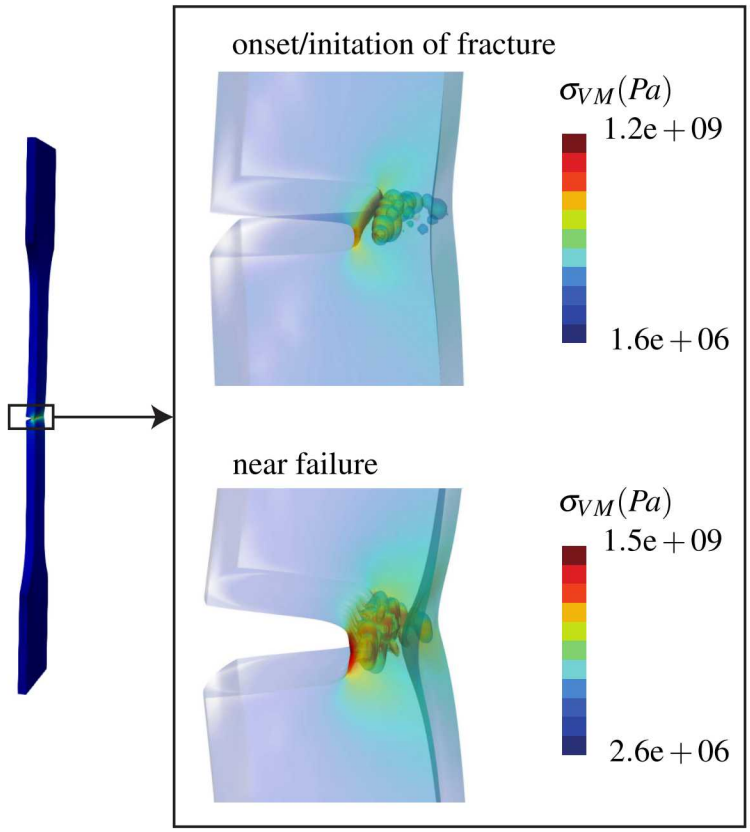

Figure 8: Von Mises stress in regions surrounding the weld at the onset of fracture (top) and near failure (bottom)

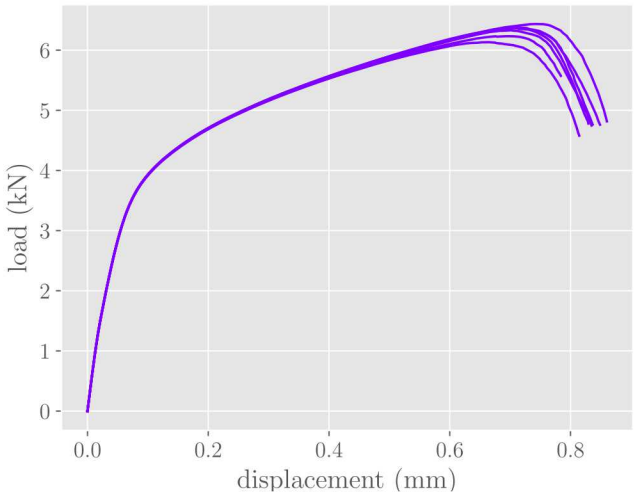

Figure 9: Force-displacement curves for the set of 10 constructed tension specimen samples

6 Verification Problem and Results

For the verification problem, a can with a radius of 1.5”, a height of 1”, a wall thickness of 0.067”, and a lid thickness of 0.062” is subjected to a localized pressure in specific areas near the edge. The weld depth is nominally 0.03” (corresponding to the size used for the traditional calibration in section 5) and is applied throughout the circumference, which attaches the lid onto the main body. The layout of the geometry is shown in fig. 10. The initial model is run using the same constitutive model parameters as those mentioned in section 5 for both the base and weld material.

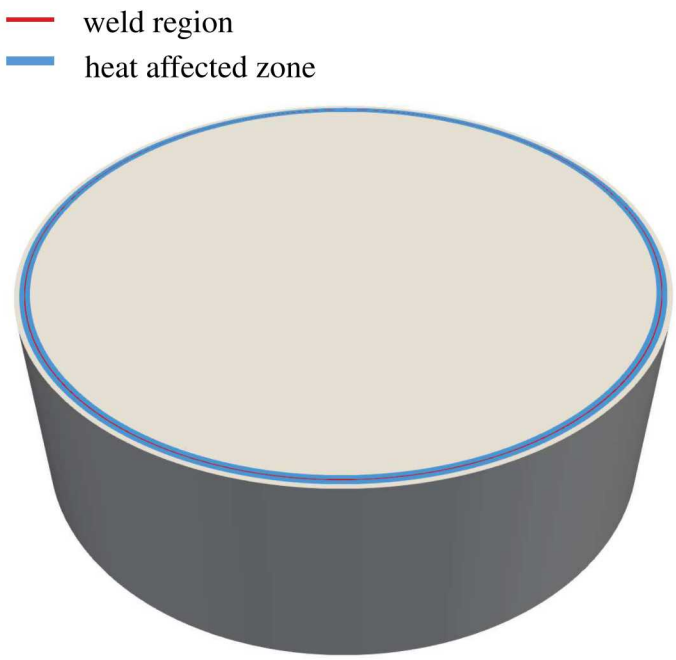

Figure 10: Overview of weld region and heat affected zone in can

A set of 60 void samples were constructed along the circumferential length of the weld, with target void volumes per unit weld plane area representative of specimens $S2$, $S4$, $S16$, $S24$, $S26$, and $S30$ (corresponding to 10 samples for each specimen). The mesh consists of approximately $2e$+06 hexahedral elements with gradual refinement near the weld. The elements at the weld region and the heat affected zone are approximately uniform with a nominal edge length of 30 μm. Symmetry is assumed along the x-, y-, and z-axes, thus reducing the total degrees of freedom by a factor of 8. The initial configuration and mesh of a single sample highlighting the void structure is shown in fig. 11. Fracture is simulated using element death/deletion as was done in section 5. The selective deviatoric element formulation was used. The locations and time evolution of the applied outward-oriented pressure within the cylinder is shown in fig. 12. The deformed shape of the cylinder at the point at which pervasive failure occurs along the weld is shown in fig. 13. The quantities of interest (QOIs) for this problem were displacements at points near the weld and at the center of the can, the total axial pressure force on the can and the time of weld breach. Quantitative results of these QOIs for the fine model are plotted with the traditional and multiscale coarse model results in section 8.3.

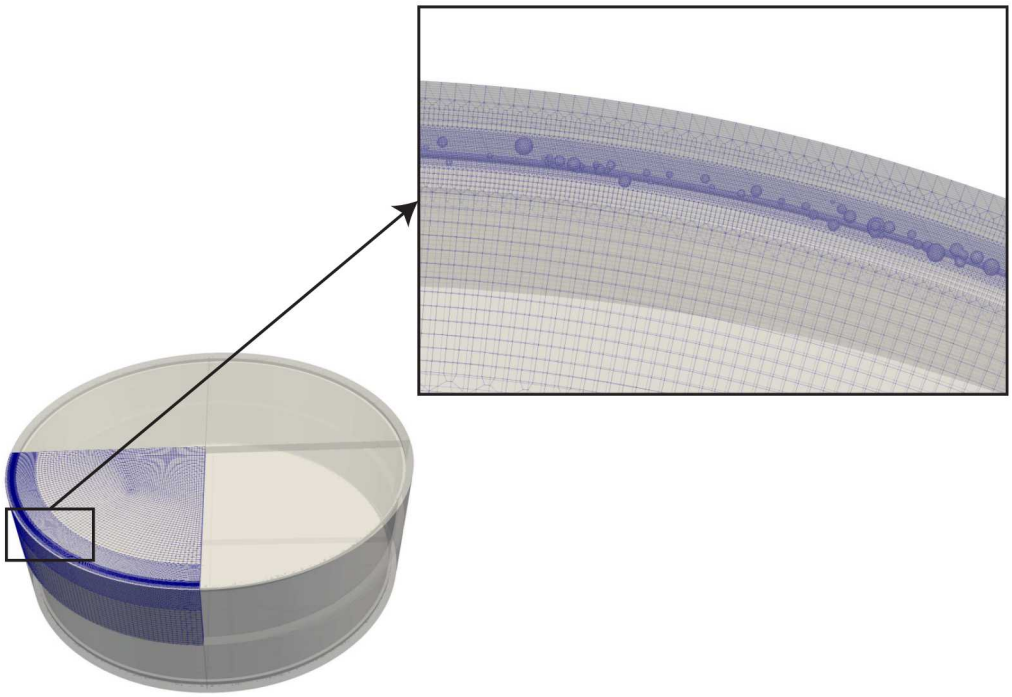

Figure 11: Mesh of can used for verification problem. Voids are shown as translucent.

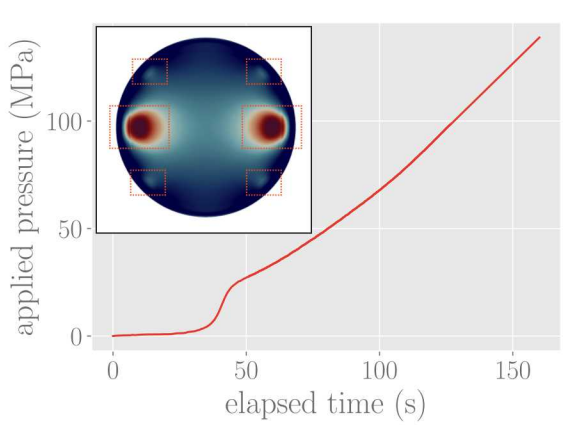

Figure 12: Magnitude of applied pressure within can as a function of elapsed time. Dashed boxed locations on contoured inset indicate where pressure is applied.

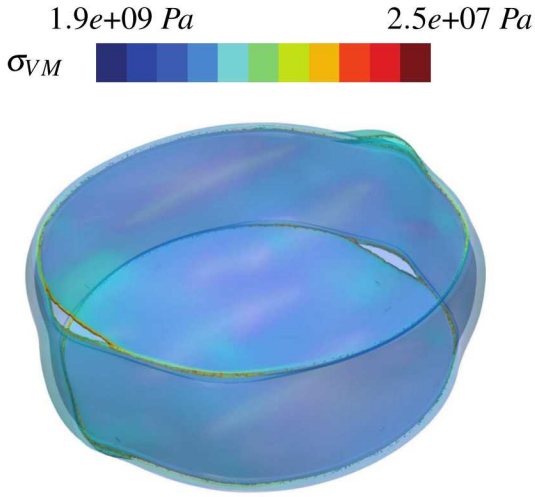

Figure 13: Pervasive failure of weld due to excessive internal pressure within can

7 Traditional Weld Failure Predictions

After all finely-meshed pressurized cans were simulated, the traditional approaches were used to predict the failure of this same model with a coarse mesh. This consisted of creating a coarse mesh

for both the tension specimens and the pressurized can, as well as developing a set of material parameters for the coarsely-meshed weld.

7.1 Coarse Model Calibration to Fine Model Weld Tension Results

The traditional coarse weld material calibration is presented here. The weld material is calibrated to the generated weld tension data from fig. 9. An image of the coarse weld tension specimen model is shown in fig. 14. Note that the timestep of 19 nanoseconds is lower than desired. The mesh could be modified to increase the stable time step of the worst element; however, for the current study, the mesh is acceptable since it is still representative of what a system analyst may use.

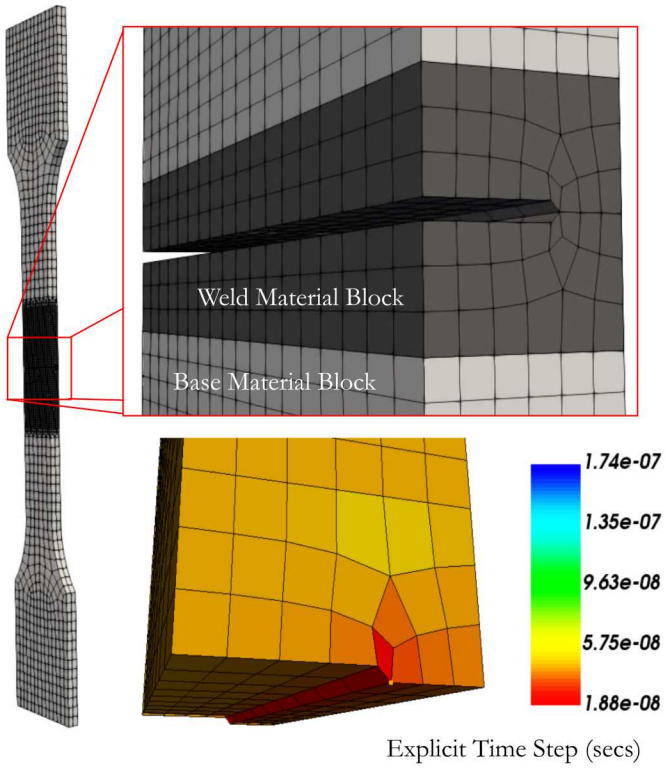

Figure 14: The coarse weld tension model is shown here. Note that the explicit time step by element is shown in the lower right. The lowest time step is about 19 nanoseconds.

Using MatCal, the material of the weld block was calibrated as an adaption of the material parameters for the base material. This adaption consisted of scaling the initial yield stress, hardening modulus and dynamic recovery parameters.The damage model was disabled in the coarse model since its mesh cannot adequately resolve the stress fields in the weld. Instead, crack initiation and failure was modeled using element deletion with a failure criterion of a critical equivalent plastic strain. As a result, four parameters were calibrated based on the force-displacement data generated by the simulation of the high-fidelity laser weld tension specimens. Two calibrations were

Table 2: Coarse weld model parameters calibrated using the traditional method.

Material Parameter	Variable	relative residual	absolute residual
Weld yield stress scale factor	Sf_Y	0.951	0.97
Weld hardening modulus scale factor	Sf_H	0.739	0.751
Weld dynamic recovery scale factor	Sf_{R_d}	2.97	2.97
Failure equivalent plastic strain	ε_f^p	1.13	1.0625

performed. The first calibration minimized the L_2-norm of the absolute residual between the generated weld tension data and coarse model data at every displacement point from the generated weld tension data. The second calibration minimized the relative residuals between the generated weld tension data and coarse model data at every displacement point from the generated weld tension data. These calibrations both yielded similar weld material parameter sets. Results from the coarse model with the two calibrated material models are plotted with the fine tension data in fig. 15. The initial point for these calibration was the base material parameters. The load-displacement results from the coarse model using the base material parameters are also shown in fig. 15. The calibrated material model parameters are given in table 2.

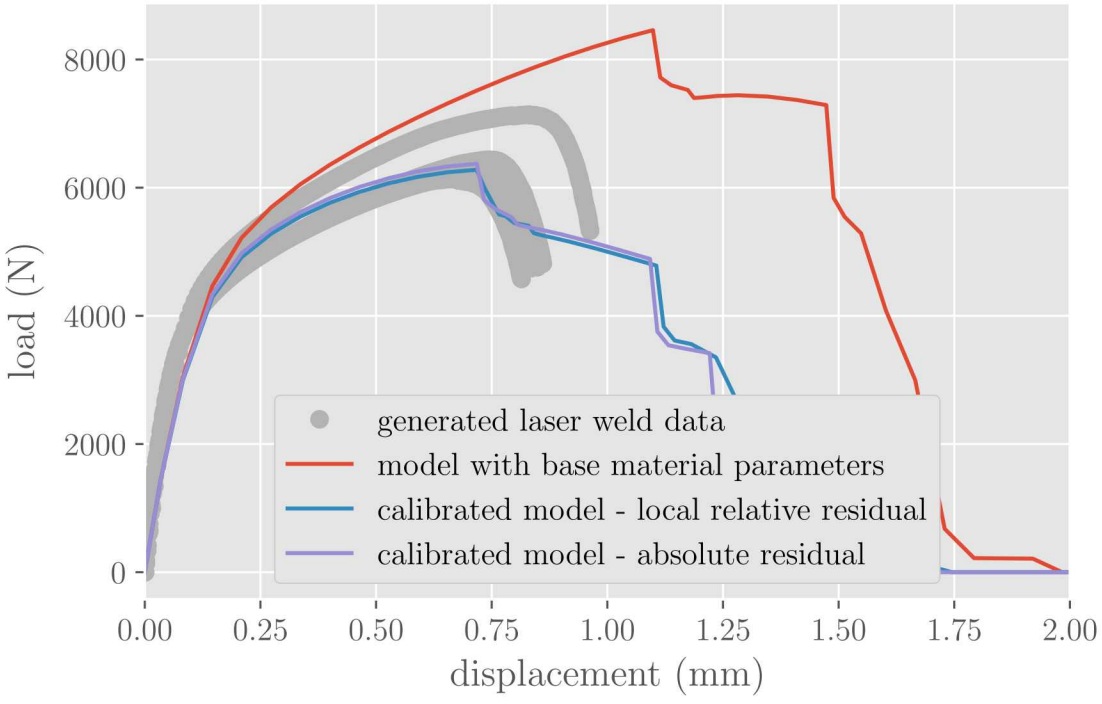

Figure 15: The load-displacement curves generated using the traditional calibration material parameters in the coarse weld tension model are shown here.

7.2 Coarse Verification Problem Prediction Using Traditional Weld Calibration

After the traditional calibration of the coarse weld model was complete, a coarse mesh of the pressurized can problem was created and the verification problem was simulated until failure. The coarse mesh of the verification problem is shown in fig. 16. A deformed mesh of the coarse verification probem simulation is shown in fig. 17. Quantitative results of the QOI's are plotted with the fine model 'truth' results and the multiscale method prediction in section 8.3. In general, the location of failure and displacement of the coarse model is similar to the fine model results.

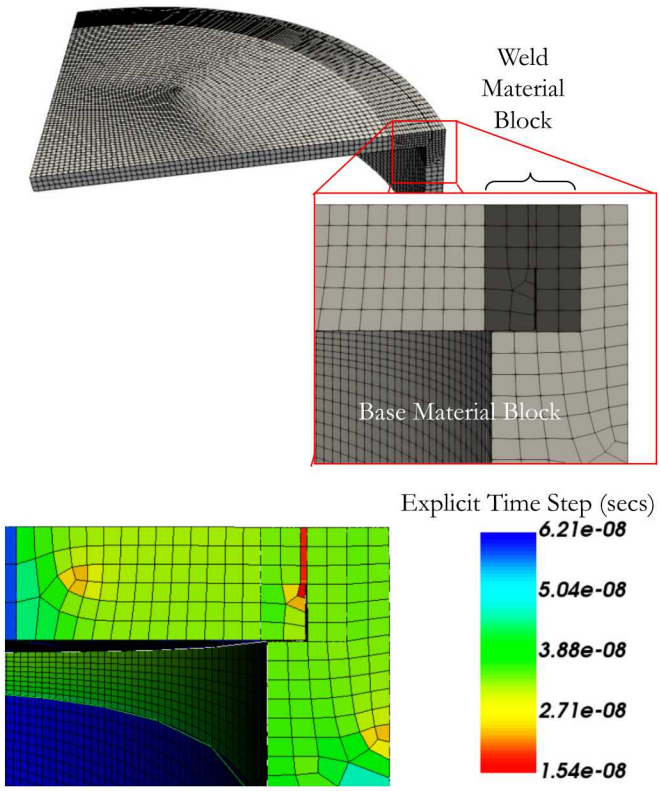

Figure 16: The coarse pressurized can model is shown here. Note that the explicit time step by element is shown in the bottom of the image. The lowest time step is about 15 nanoseconds.

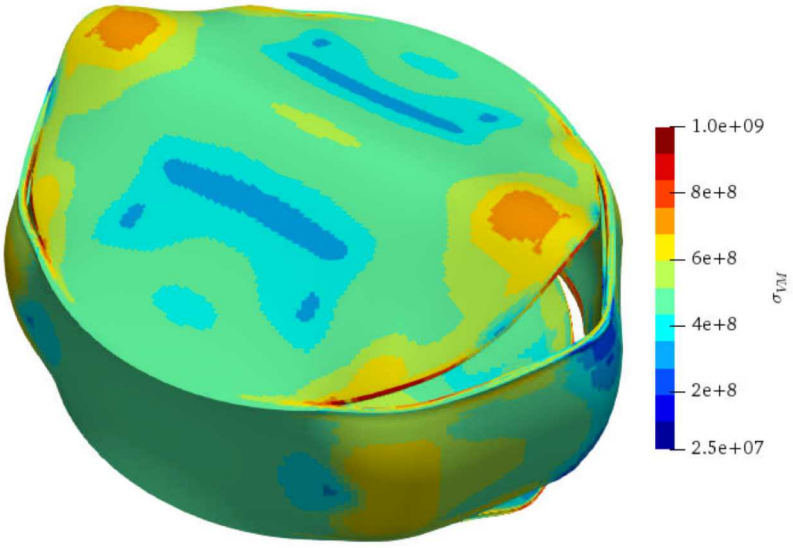

Figure 17: The deformed coarse pressurized can model is shown here. The coarse model was able to run until the lid completely seperated from the cylinder of the can.

8 Multiscale Modeling of the Verification Problem Weld

8.1 Fine Model Submodeling of Weld Region

Traditionally, material calibrations of welds are performed by optimizing a set of parameters for a given constitutive law based on a known set of response data, such as the force-displacement relation of a uniaxially loaded tension specimen (this provides the basis of the results presented in section 5). However, there is no guarantee that the material response is independent of the actual loading and geometry of any given laser-welded specimen with the same nominal weld depth. When performing a material calibration for the weld along the circumference of the can used in sections 6 and 7, it is thus desirable to account for the pertinent loading and geometry in the input.

Within the context of the verification problem discussed in sections 6 and 7, we extract 9 subregions along the circumference of the weld which are approximately 0.1” in length, 0.05” in width and 0.063” in height, as shown in fig. 18. A total of 60 sets of voids are constructed based on the same target void volume fractions used in section 6. Each subvolume is meshed with approximately $90k$ hexahedral elements, which have nominal edge lengths of $30\mu m$. These subvolumes serve as representative samples of the fine features that control the global properties of the full pressurized can. With this in mind, the subvolumes are used as calibration specimens from which material parameters can be estimated for the problem-at-hand. To accomplish this task, the displacements experienced by the original coarsely-meshed model are applied on the surfaces of the subvolumes where they intersect. An example illustrating this concept is shown in fig. 19. To capture the effects of the inclusion of voids, the time evolution of the resultant forces on the surfaces intersecting the original can are used to re-calibrate the material parameters. This procedure is discussed in greater detail below.

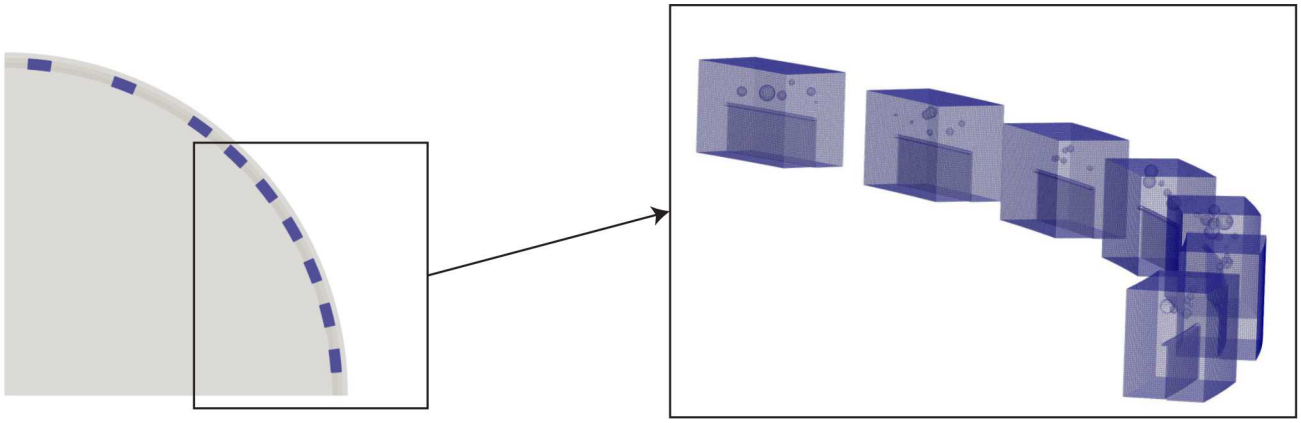

Figure 18: Mesh of subregions of interest along weld of can used for fine-scale-informed material calibration. Voids are shown as translucent.

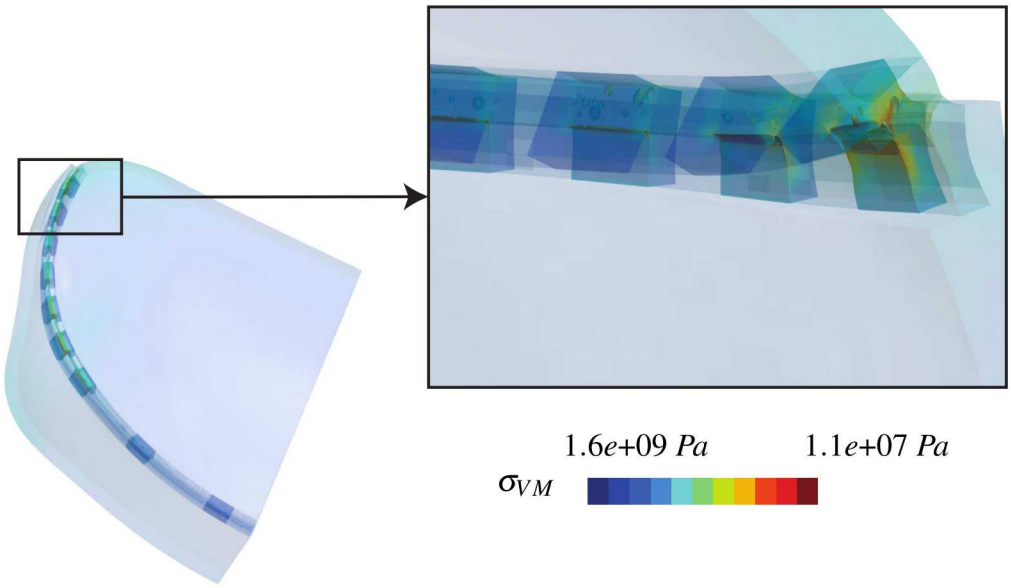

Figure 19: Subvolume deformation induced by applied displacements occurring on the coarsely-meshed can

8.2 Calibrating Coarse Subvolumes Model to Fine Subvolumes Model Results

After simulating the fine subvolumes, a coarse mesh was made for the subvolumes and the weld material model was calibrated to the fine subvolume simulation results. Specifically, the resultant force time history from every boundary condition surface of the coarse subvolumes model was calibrated to the resultant force time history of the corresponding surface from the fine subvolumes model. The resultant force described here is the resultant force vector magnitude on each surface and does not include the resultant torque. With 60 subvolume realization simulations and 45 resultant force ouput for each realizations, each objective function evaluation required the evaluation

Table 3: Coarse weld model parameters calibrated using the proposed hierarchical multiscale method.

Material Parameter	relative residual	absolute residual	combined residual
Sf_Y	0.781	0.845	0.804
Sf_H	0.627	0.296	0.479
Sf_{R_d}	2.61	0.963	2.31
ε_f^p	1.75	1.36	1.75

of 2700 residual vectors when calibrating to all subvolumes. This is the type of calibration where a tool like MatCal is needed to ensure success and completion in a timely manner. The MatCal calibration process for the coarse subvolumes model was as follows:

1. Simulate the coarse subvolumes model with the coarse weld material parameter set from the tradiational calibration. Discard force time histories where model form error for the coarse model is large.

2. Calibrate the plasticity parameters of the coarse weld model (Sf_Y, Sf_H, Sf_{R_d}) to the fine subvolumes model results from time 90 to 140 seconds. This time frame was chosen because the response of the subvolumes is dominated by plasticity over this period.

3. With the plasticity parameters from the previous step, calibrate ε_f^p to the fine subvolumes model results from time 150 to 152 seconds. This time frame was chosen because the response of the subvolumes is dominated by crack growth over this period. Note that only the results from the subvolume that was experiencing crack growth was used for this part of the calibration.

The above calibration procedure for the plasticity parameters was repeated for the relative residual and absolute residual as was done for the traditional coarse weld model calibration. An additional calibration was also done using an equally weighted average of the relative residuals and absolute residuals which we will refer to as the combined residual calibration. For the damage calibration step, only the absolute residual was used for calibration. In general, the surfaces that had their normal vectors aligned with the weld arc (right and left side surfaces) and the surfaces on the outer cylinder edge (outer surfaces) were discarded due to model form error. An example of the model form error for the right and outer surfaces are shown in fig. 20. Results generated using coarse models calibrated with the multiscale method are shown for subvolume 1, the subvolume in the region of initial failure, in fig. 20 and fig. 22. Results generated using coarse models calibrated with the multiscale method are shown for subvolume 2, the subvolume next down the weld length, in fig. 21. The other subvolumes show similar results so these plots are excluded for the sake of brevity. The three calibrated material parameter sets are given in table 3

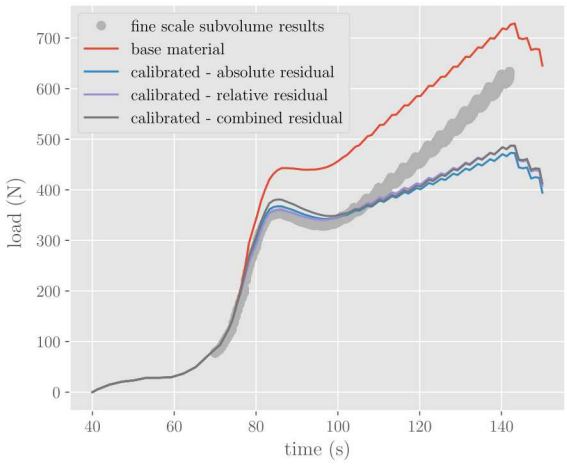

(a) bottom surface of subvolume 1

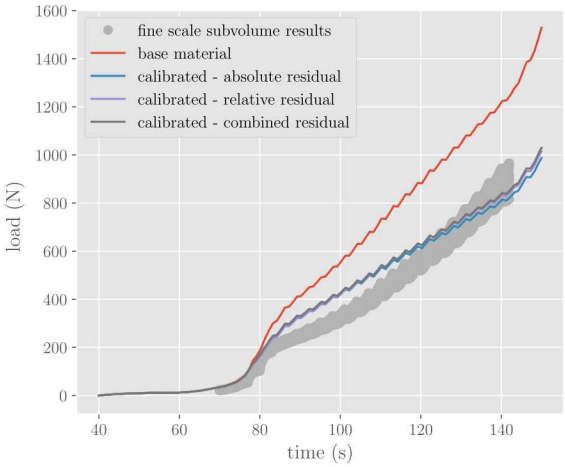

(b) inner surface of subvolume 1

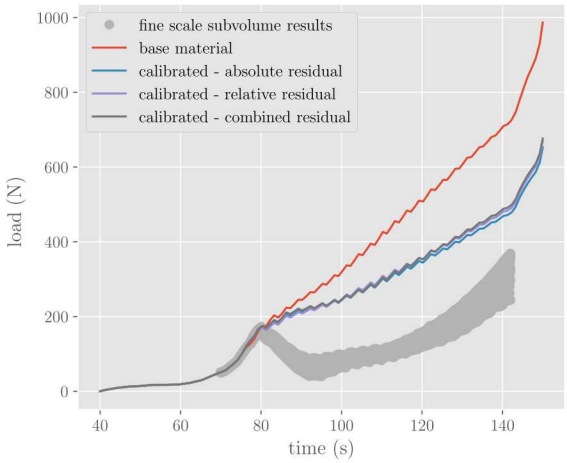

(c) outer surface of subvolume 1 (discarded/not calibrated)

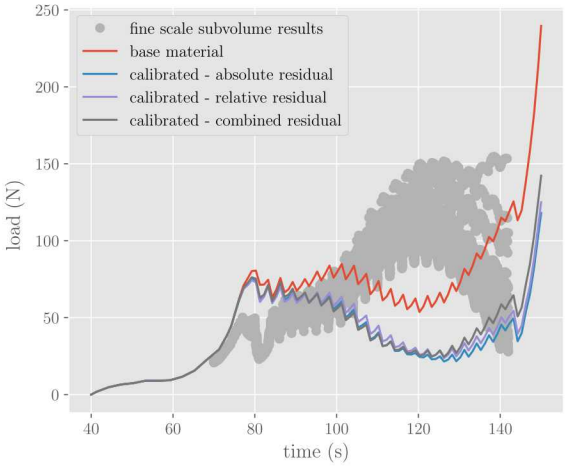

(d) right surface of subvolume 1 (discarded/not calibrated)

Figure 20: Plasticity calibration results for the coarse subvolumes model are shown here for the hierarchical multiscale calibration method.

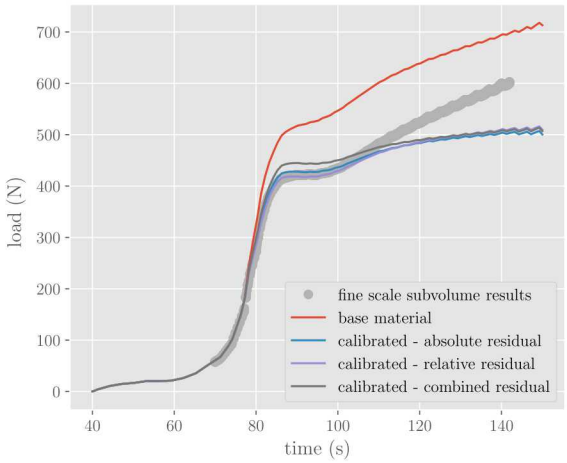

(a) bottom surface of subvolume 2

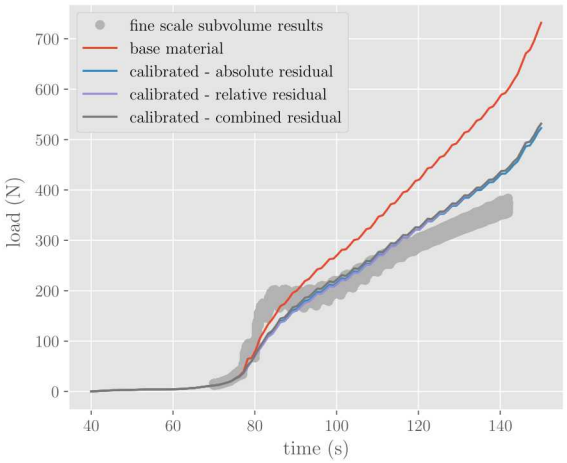

(b) inner surface of subvolume 2

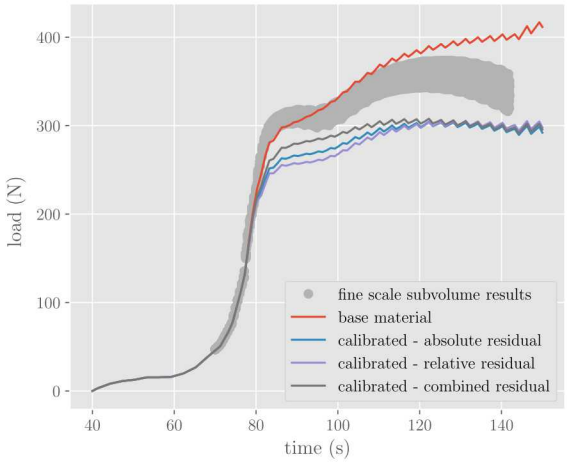

(c) outer surface of subvolume 2

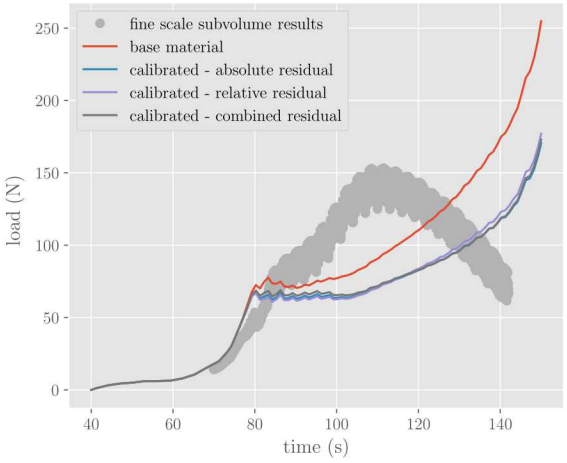

(d) right surface of subvolume 2 (discarded/not calibrated)

Figure 21: Plasticity calibration results for the coarse subvolumes model are shown here for the hierarchical multiscale calibration method.

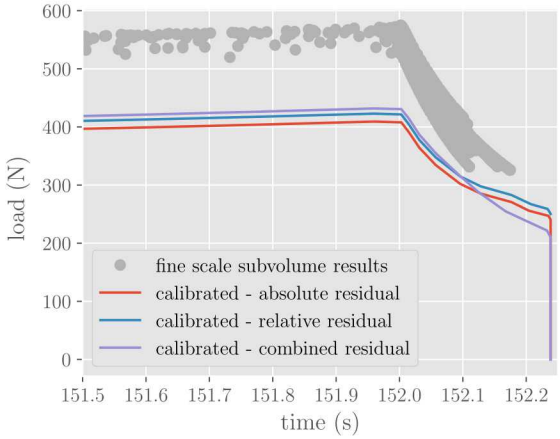

(a) bottom surface of subvolume 1

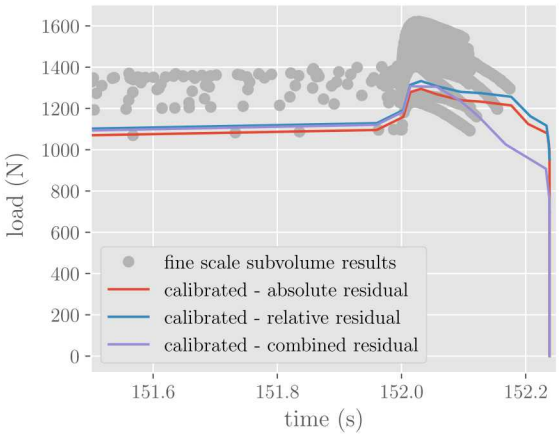

(b) inner surface of subvolume 1

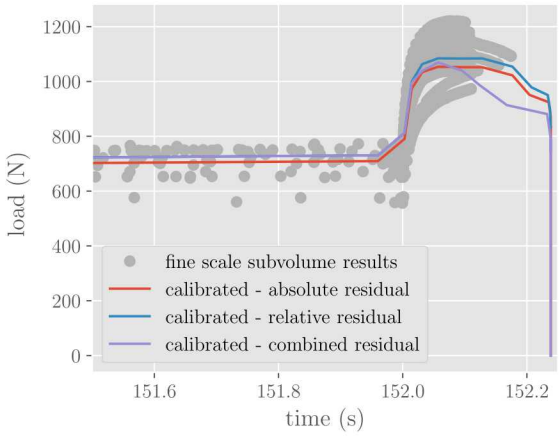

(c) outer surface of subvolume 1

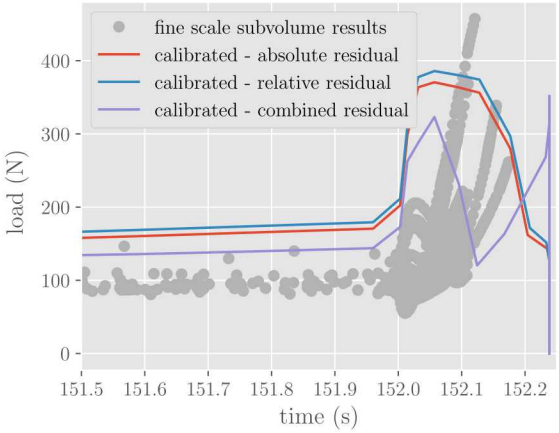

(d) right surface of subvolume 1 (discarded/not calibrated)

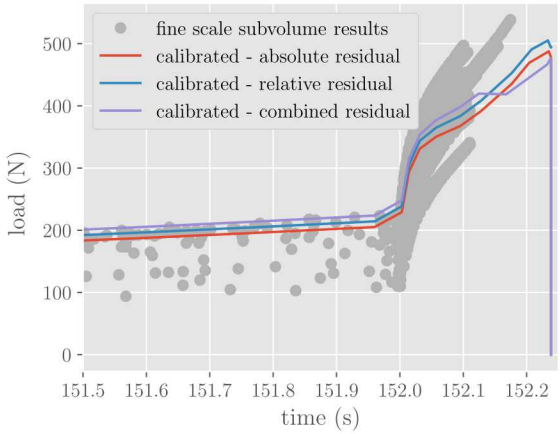

(e) left surface of subvolume 1

Figure 22: Failure calibration results for the coarse subvolumes model are shown here for the hierarchical multiscale calibration method.

8.3 Updating Coarse Model Predictions and Comparing Traditional Method Predictions

The coarse model predictions were compared to the fine model results for every QOI. The QOIs include displacements at the points shown in fig. 23, the time of breach of the weld and the force in the axial direction of the can (referred to as the vertical force). The vertical force history and load-displacement curves for each point are compared in figs. 24 to 29. The displacement is the total displacement magnitude at the location being monitored for the given applied pressure.

All the simulation curves were interpolated to common points, so that global error metrics could be calculated for each coarse model. Similar to the different treatments of residuals for the calibrations, a local residual and an absolute residual were used for the global error metric calculation. The global error metric was then calculated as the L_2-norm of the combined residual vector for the coarse model compared to every fine simulation result that had the vertical load drop by 45%. As a result, the global error metrics only include comparison to 14 fine models because not all fine model reached this amount of crack growth and load drop. Additionally, the residual vector for each coarse model includes the force errors for all 5 displacement locations being monitored. The absolute residuals are normalized by the average load for each curve included in the residual vector. The error in the time of failure is calculated with respect to the average failure time of the fine models. The displacements were monitored at points that could be considered global deformation metrics (location 1) and local deformation metrics near the weld (location 2, 3, 4 5). As a result, the global error metrics should be representative of the error in overall deformation and crack length for the models. The global error metrics for each coarse model are reported in table 4.

In general, the coarse models calibrated using the multiscale method quantitatively make more accurate predictions according our global error metrics. Particularly the multiscale method produce a more accurate prediction of the failure time and deformation after failure. It is worth mentioning that the traditionally calibrated coarse models also perform fairly well. However, the multiscale informed models do perform better for predicting post-failure behavior. Qualitatively, the coarse models calibrated using the multiscale method under predict the structural compliance of the can post-peak load, but more accurately capture the load and displacements while the crack is growing. The coarse models calibrated using the traditional method generally under predict the load post-failure, but are more accurate in modeling the structural compliance of the can pre-peak load.

Table 4: Global error metrics for comparing the coarse model results to the fine model results they are attempting to predict.

Coarse Model Calibration Method	**Global Error Relative Residual**	**Global Error Absolute Residual**	**Failure Time Error (%)**
base material	92.5	119.7	16
traditional absolute residual	27.2	36.4	-4.5
traditional relative residual	34.1	44.7	-3.7
multiscale absolute residual	24.6	32.1	-1.7
multiscale relative residual	23.5	30.3	2.2
multiscale combined residual	20.2	26.1	0.14

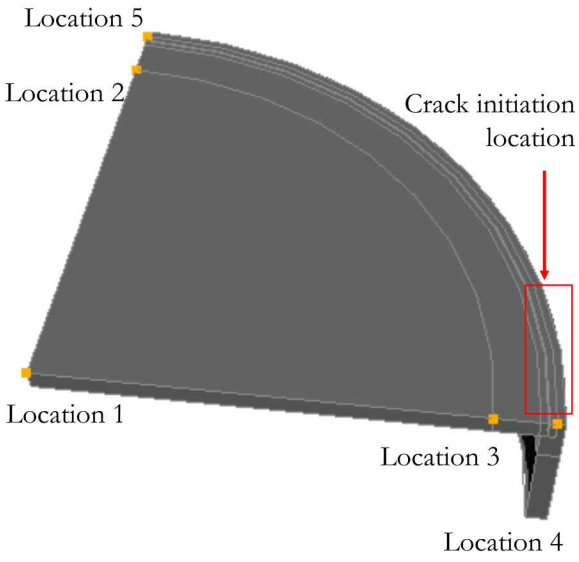

Figure 23: Locations where displacements are extracted for model verification.

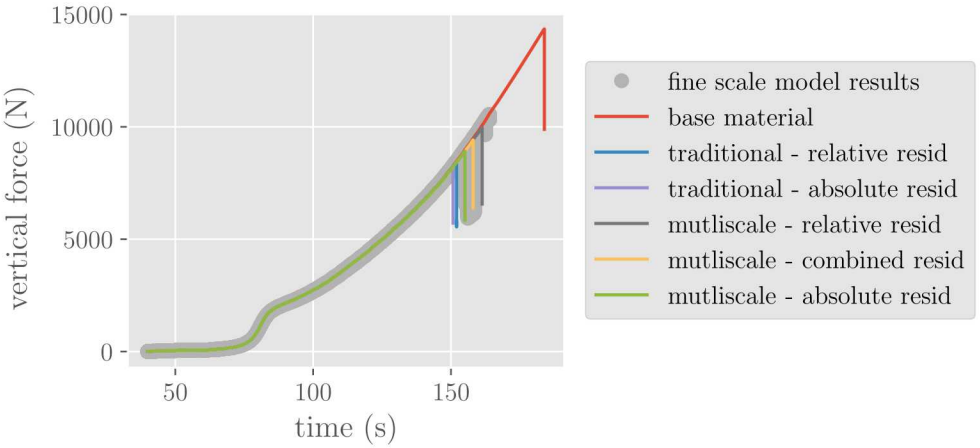

Figure 24: Coarse model predictions compared to the fine model results for the vertical force history.

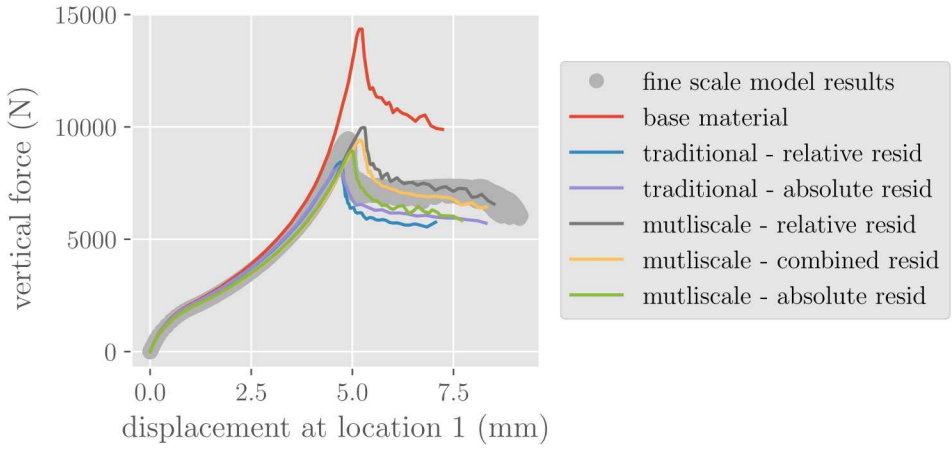

Figure 25: Coarse model predictions compared to the fine model results for the displacement magnitude at location 1.

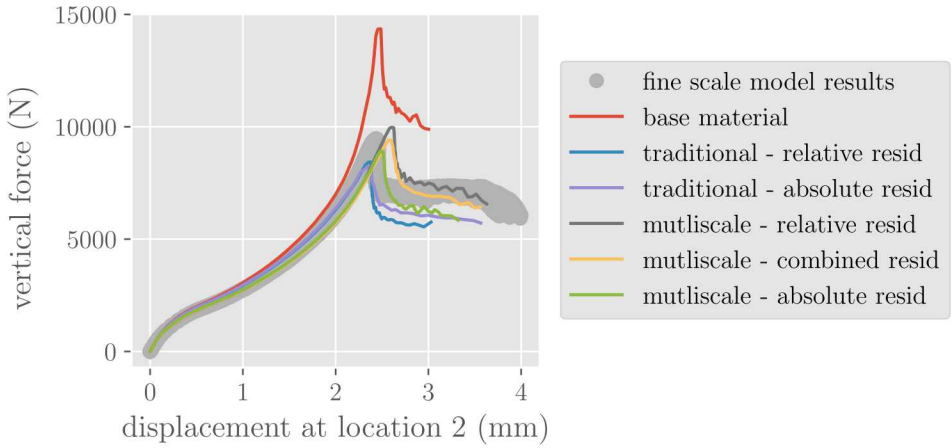

Figure 26: Coarse model predictions compared to the fine model results for the displacement magnitude at location 2.

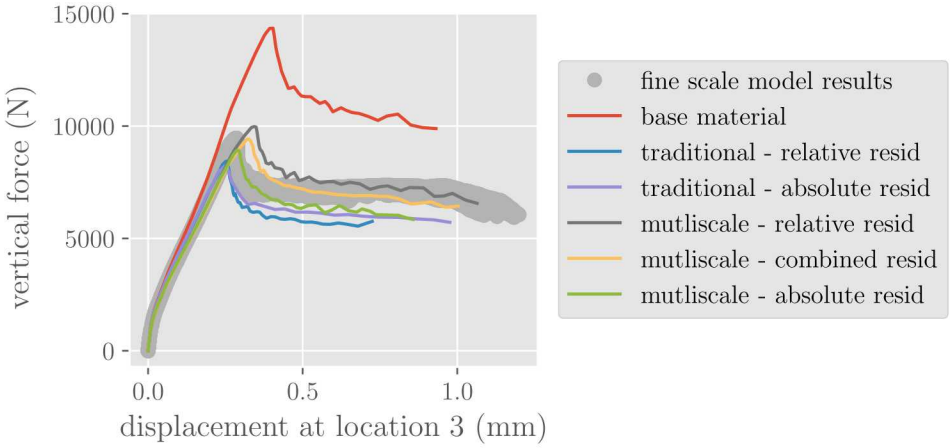

Figure 27: Coarse model predictions compared to the fine model results for the displacement magnitude at location 3.

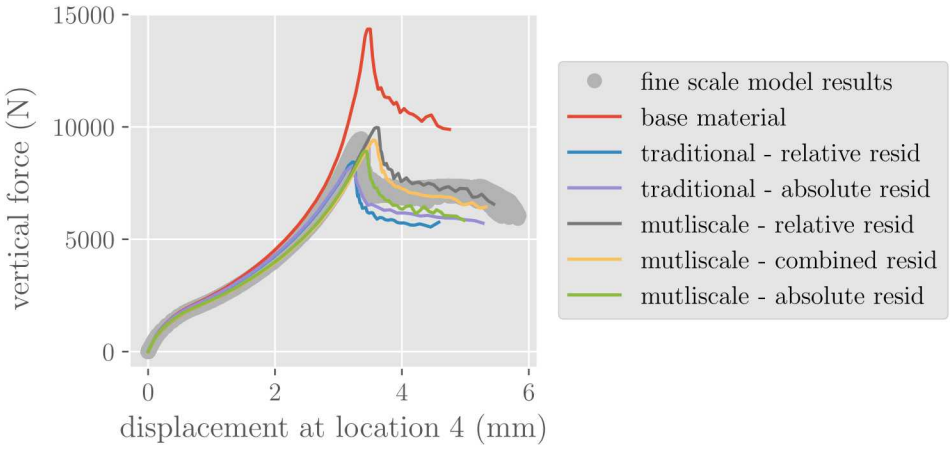

Figure 28: Coarse model predictions compared to the fine model results for the displacement magnitude at location 4.

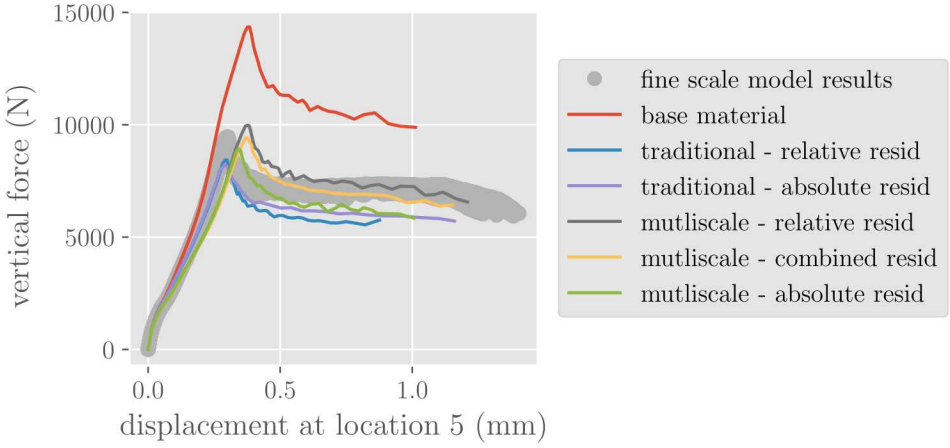

Figure 29: Coarse model predictions compared to the fine model results for the displacement magnitude at location 5.

9 Conclusions

Overall, coarse models calibrated using both the traditional and multiscale calibration methods performed well at predicting the failure of the fine model pressurized can. However, the coarse models calibrated with the multiscale method performed notably better according to our global quantitative error metrics. They were also better at predicting the loads and deformation through crack initiation and propagation.

It should be noted that the multiscale informed coarse model calibration method does have room for improvement. In general, the coarse models calibrated using the mutliscale method were too compliant pre-peak load, while the traditionally calibrated coarse models did well pre-peak load. We think this may be due to model form error of the coarse subvolume model and the additional constraint on the suvolumes due to their poor discretization and small size. We think this constraint was less of an issue with the traditional calibration coarse model because the boundary condition is applied far away. Another issue with the multiscale informed coarse models is that the calibrated coarse model parameters are fairly sensitive to the residual and other options used for the calibration. This sensitivity to calibration options is not seen for the traditional calibration. To remedy both of these issues will require looking at different metrics for calibrating the subvolumes models and varying the size and selection of the subvolumes themselves. For example, we could calibrate to the internal force across the weld plane for each subvolume instead of the force on every external surface as was done here. Also, we could extend the subvolumes into the base material to reduce the constraint of the prescribed boundary conditions on the small subvolumes with a coarse mesh.

Future work will consist of:

1. Examining different subvolume calibration metrics.
2. Examining the effect of subvolume size.
3. Examining sensitivity to subvolume discretization. These discretizations will still be considered coarse but the meshes will be more tailored than those studies here.
4. Examining the effect of different material models for the coarse model (e.g. MLEP, cohesive zone elements, etc.)
5. Determining the cause of the oscillations seen in the subvolume force-time curves as seen in figs. 20 and 21.
6. Verify the method on a problem with more stable crack growth and use the modular material model for the fine model. The current fine model uses DSA which was not reliable for every simulated geometry.
7. Validate the methods against experimental tests of components with welds that have proper characterization data.

In summary, we believe these results show that the multiscale subvolume approach shows promise for improving laser weld failure predictions in system and component models. They also suggest that hierarchical multiscale modeling can be used to improve laser weld failure modeling by providing generated data for the traditional type calibration. For example, the fine models can be used in the traditional calibration approach if test data for welds is not available but geometric parameters are. This could be the case if as-produced welds are different than those tested in a lab or if structural testing has not been conducted on the weld of interest. Note that both of these hierarchical multiscale methods require a quality material model for the fine model and CT scan characterization of laser weld geometries. Without this data to build the fine model, accurate predictions cannot be made.

Note that the trends in the coarse model results should not be given too much weight. Specifically, for this case the coarse models for the traditional calibration method appear to be more conservative as they failure earlier than the fine model. We stress that the conservatism or unconservatism of a given calibration method cannot be guaranteed. Also, the conservatism of a response depends on the model being evaluated because in some scenarios a weld failing later may be more conservative.

10 Acknowledgments

Sandia National Laboratories is a multimission laboratory managed and operated by National Technology and Engineering Solutions of Sandia, LLC., a wholly owned subsidiary of Honeywell International, Inc., for the U.S. Department of Energy's National Nuclear Security Administration under contract DE-NA-0003525.

This work describes objective technical results and analysis. Any subjective views or opinions that might be expressed in the paper do not necessarily represent the views of the U.S. Department of Energy or the United States Government.

References

[1] United States. Federal Aviation Administration, Battelle Memorial Institute. Columbus Laboratories, William J. Hughes Technical Center (U.S.), United States. Department of Defense, United States. National Aeronautics, and Space Administration. *Metallic Materials Properties Development and Standardization (MMPDS): MMPDS-10*. Federal Aviation Administration, 2015.

[2] Coleman N. Alleman, James W. Foulk, Iii, Alejandro Mota, Hojun Lim, and David J. Littlewood. Concurrent multiscale modeling of microstructural effects on localization behavior in finite deformation solid mechanics. *Comput. Mech.*, 61(1-2):207–218, February 2018.

[3] Arthur A. Brown and Douglas J. Bammann. Validation of a model for static and dynamic recrystallization in metals. *International Journal of Plasticity*, 32-33:17–35, 2012.

[4] Kyle Karlson, Coleman Alleman, Corbett Battaile, Guy Leshem Bergel, Brad Boyce, John Emery, James Foulk, Alexander Hanson, Huiqing Jin, Sharlotte

Kramer, and Alyssa Madison, Jonathanand Skulborstad. 304l ss laser weld failure model development and validation. Number SAND2019-8318PE. Sandia National Labs. https://digitalmedia.sandia.gov/Mediasite/Showcase/digital-media/Presentation/a53a31fe643d48449b1c78d6056530b51d.

[5] Sharlotte Kramer. Characterization of 304l stainless steel laser welds. SAND Report SAND2015-9012, Sandia National Laboratories, Albuquerque, NM, 2015.

[6] Alejandro Mota, Irina Tezaur, and Coleman Alleman. The schwarz alternating method in solid mechanics. *Computer Methods in Applied Mechanics and Engineering*, 319:19 – 51, 2017.

[7] Hans Nordberg. Note on the sensitivity of stainless steels to strain rate. Research Report 04.0-1, AvestaPolarit Research Foundation and Sheffield Hallam University, 2004.

[8] SIERRA Solid Mechanics Team. Sierra/SolidMechanics 4.52 theory manual. SAND Report SAND2019-2714, Sandia National Laboratories, Albuquerque, NM and Livermore, CA, 2019.

[9] SIERRA Solid Mechanics Team. Sierra/SolidMechanics 4.52 User's Guide. SAND Report SAND2019-2715, Sandia National Laboratories, Albuquerque, NM and Livermore, CA, 2019.

Internal Distribution:

MS-0825	Shawn Burns	Org. 1514
MS-9042	Mike Veilleux	Org. 1542
MS-0840	Edmundo Corona	Org. 1554
MS-1133	Brian Lester	Org. 1554
MS-9042	Jon Madison	Org. 1851
MS-9042	Alejandro Mota	Org. 8363
MS-9042	Jake Ostien	Org. 8363
MS-9042	Matt Kury	Org. 8751
MS-9042	Guy Bergel	Org. 8752
MS-9042	Jay Dike	Org. 8752
MS-9042	Gabriel de Frias	Org. 8752
MS-9042	Stacy Nelson	Org. 8752
MS-9042	Alyssa Skulborstad	Org. 8752